

A Direct Two-Dimensional Pressure Formulation in Molecular Dynamics

Sumith Yesudasan^{a,1} and Sibi Chacko^b

^aSchool of Chemical, Materials, and Biomedical Engineering, University of Georgia, Athens, Georgia 30606, USA; ^bSchool of Engineering and, Physical Science, Heriot Watt University, Dubai Campus, Dubai, UAE 294345

This manuscript was compiled on February 27, 2022

Coupling of statistical properties from atomistic simulations to continuum is essential to model many multi-scale phenomena. Often, the system under consideration will be homogeneous in two-dimensions (2-D). But due to the existing coupling methods, the property estimation takes place in three-dimensions (3-D) and then averaged to 2-D, which is computationally expensive due to the 3-D convolutions. A direct 2-D pressure or stress estimation model is lacking in literature. In this work, we develop a direct 2-D pressure field estimation method which is much faster than 3-D methods without losing accuracy. The method is validated with MD simulations on two systems: a liquid film and a cylindrical drop of argon suspended in surrounding vapor. This formulation will enable the study of 2-D fundamental phenomena like passive liquid flows in microlayer, as well as facilitate the coupling of atomistic and continuum simulations with reduced computational cost.

Molecular dynamics | Local pressure | Multiscale coupling

Multi-scale coupling of atomistic and continuum simulations is of significant importance in the areas of heat transfer, fracture mechanics and bioengineering (1). For example, in the study of bio-membrane bending, it is necessary to understand the local variations of pressure and stress which are inaccessible through experiments (2–5). These computations typically map properties determined from atomistic simulations onto grid points in continuum simulations (6), which is used for estimating interfacial energies, surface tension, pressure gradients in fluid simulations and lipid bilayer mechanics. Many simulated systems have inhomogeneity only in two dimensions (2-D) such as defect nucleation in bulk and 2-D crystals, bio molecular assemblies such as lipid bilayers and membrane proteins, as well as thin film evaporation and heat transfer (7–9), and thus only require 2-D pressure distribution. However, current literature on local pressure estimation is based on 3-D (10) or 1-D (11–13) pressure estimation. The 2-D pressure distribution is obtained by averaging over the 3-D pressure data, and is extremely computationally expensive (14) as it involves a 3-D convolution. A generalized method for 3-D stress calculations which included temporal averaging weight functions was derived by Yang (15). Recently, Vanegas (14) and Sanchez et al. (16) applied the modified Hardy versions of IK stress to lipid bilayers, coiled coil protein and graphene sheet to determine continuum level properties from atomistic simulations. Further, there exist a few Irving-Kirkwood versions (17–19) of 1-D pressure calculations for 1-D inhomogeneous system. However, to the best of our knowledge, no methods are present for a direct 2-D pressure estimation.

This work presents a 2-D pressure estimation algorithm based on Hardy’s stress method, which is validated by performing molecular simulations of a suspended liquid film and a cylindrical drop and comparing the results with experimental

data and classical Young-Laplace equation, respectively. This can be very useful not only in atomic scale systems but also in mesoscale dynamics with continuum coupling (20–23).

Historically, the atomic level virial stresses from statistical analysis were first derived by Irving and Kirkwood (24), now generally referred to as IK method. The need for large ensemble averaging due to the delta function in IK method was circumvented by Hardy in his classical paper (19, 25) by introducing a smoothing function and a bond function. The virial stress has two components, a kinetic component and a force component. There existed an ambiguity among researchers about the equivalence of virial stress with Cauchy stress. The ambiguity is thoroughly discussed in Zhou’s paper (26) which claims that Cauchy stress is not equivalent to virial stress, but is equivalent only to the force component of virial stress. Based on this finding, researchers (27–30) performed a number of molecular studies. Zimmerman (27) showed that, for crystals, Hardy’s stress formulation gave more accurate results than simple local virial averages. A comparative study of different versions of local virial stress was studied by Murdoch (31). In contrast to Zhou’s work (26), Subramaniyan (32) found that virial stress is indeed the Cauchy stress using specific examples. There were other works (33, 34) which tried to develop the appropriate relation of virial stress and continuum level stresses.

All these studies are performed in 3-D domain and later averaged to 2-D. A consistent direct 2-D formulation of local pressure is missing in the literature. In this paper we will derive 3-D, 2-D and 1-D versions of local pressure estimation. This will be used to estimate pressure, density and temperature of certain case studies and will be validated. Our work also supports the fact that while converting virial stress to a continuum level property, both kinetic component and force component of virial stress should be considered.

Local pressure estimation. The 3-D pressure from molecular interactions is estimated classically by IK method (24) through the expression shown in Eq. 1. Here, the first term represents

Significance Statement

This paper presents an accurate mathematical method to estimate the pressure in an atomic system on a two dimensional plane. This method can replace the traditional three dimensional estimation of pressure and then averaging to a 2D grid and hence can save computational power.

All authors equally contributed

Authors have no conflicts of interests to declare

¹To whom correspondence should be addressed. E-mail: sumith.yd@uga.edu

the kinetic energy contribution and second represents the virial contribution.

$$P(r_p) = P_K(r_p) + P_V(r_p) \quad [1]$$

Kinetic contribution is,

$$P_K(r_p) = \sum_{i=1}^N m_i v_i \otimes v_i \delta(r_i - r_p) \quad [2]$$

Virial contribution is

$$P_V(r_p) = \sum_{i=1}^{N-1} \sum_{j=i+1}^N r_{ij} \otimes F_{ij} \delta(r_i - r_j) \delta(r_i - r_p) \quad [3]$$

Here P is the pressure, m is mass of i^{th} atom, v is velocity, r_i and r_j are the position vectors of i^{th} and j^{th} atoms respectively, N is number of atoms, r_p is the position vector of p^{th} grid point, $r_{ij} = r_i - r_j$, F_{ij} is the force, and δ is the Dirac delta function (35). Though this expression is theoretically correct, practically it needs infinite sampling, which makes it less appealing for finite computer simulations. Specifically, for molecular dynamics simulations this is computationally expensive due to its convolution nature. To evade this situation, Hardy introduced (19, 25) interpolation functions to distribute the kinetic contribution and a bond function to distribute the virial contribution to the local grid points. This resulted in the modified expression for pressure as

$$P(r_p) = \sum_{i=1}^N m_i v_i \otimes v_i w(r_i - r_p) + \sum_{i=1}^{N-1} \sum_{j=i+1}^N r_{ij} \otimes F_{ij} B_{ij}(r_p) \quad [4]$$

Here, w is the weight function (interpolation function) and B is the bond function and defined as

$$B_{ij}(r_p) = \int_0^1 w(\lambda r_{ij} + r_i - r_p) d\lambda \quad [5]$$

A weight function has to be normalized and should follow

$$\int_{R^3} w(r) dr^3 = 1 \quad [6]$$

3-D pressure formulation. For a 3-D system, if the distribution is assumed to be spherically symmetric, then

$$\int_{R^3} w(r) dr^3 = \int_0^\infty \hat{w}(r) 4\pi r^2 dr = 1 \quad [7]$$

If the spread of the function is limited to a certain spread radius r_s then the equation becomes

$$\int_{R^3} w(r) dr^3 = \int_0^{r_s} \hat{w}(r) 4\pi r^2 dr = 1 \quad [8]$$

Here, $\hat{w}(r)$ is the weight function and used by researchers (15, 33) for 3-D grid, is given as:

$$\hat{w}(r) = C_1 [1 - 3r^2/r_s^2 + 2r^3/r_s^3] \quad [9]$$

here, C_1 is the normalization constant. For 3-D systems,

$$\int_{R^3} w(r) dr^3 = \int_0^{r_s} 4\pi r^2 C_1 [1 - 3r^2/r_s^2 + 2r^3/r_s^3] dr = 1 \quad [10]$$

the constant of integration takes the form $C_1 = 15/4\pi r_s^3$ and $r(x, y, z)$ is a function in three coordinates.

2-D pressure formulation. In this section we will explain the formulation of 2-D local pressure method by reformulating the 3-D weight function which will significantly reduce the computational cost without losing any desired details in the results. Typically, a 3-D local pressure method requires $N^2 \times N_X \times N_Y \times N_Z \times N_B$ operations (N is the number of atoms; N_X , N_Y and N_Z are the number of grid points along x, y and z-directions respectively; N_B is the number of discrete points for bond function integration). Here, the first term N^2 is the cost of inter-atomic pair potential force determination, which can be reduced to $O(N)$ using cell list algorithms (36). This will make the 3-D pressure estimation cost as $N \times N_X \times N_Y \times N_Z \times N_B$ as shown in the Fig. 1a.

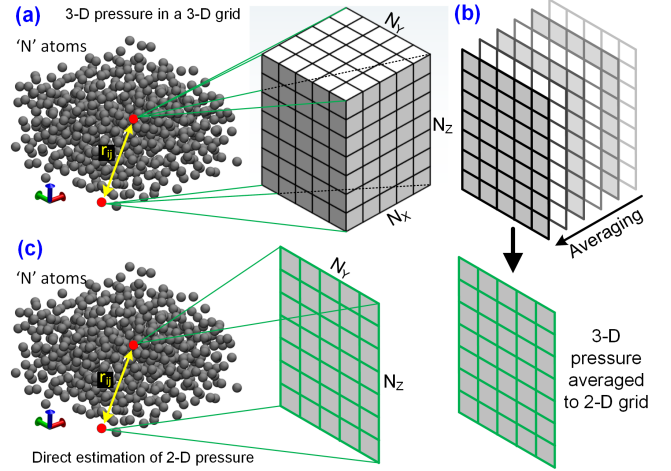


Fig. 1. Local pressure estimation in 3-D and 2-D grids. (a) Schematic of pressure estimation in a 3-D grid from a molecular system. (b) Estimation of pressure in a 2-D grid by averaging the 3-D grid data (This is the traditional approach). (c) Direct estimation of pressure in 2-D grids from the MD simulation system (this work).

While estimating the pressure in a 2-D grid, traditionally, the pressure in the 3-D grid is averaged to obtain it as seen in the Fig. 1b. This expensive step will become unnecessary if we can directly estimate the pressure in 2-D grids as shown in Fig. 1c. Though it looks like a trivial case, the results are very promising by reducing the computational effort to $N \times N_X \times N_Z \times N_B$. In this work, we propose that while extending the pressure estimation theory to a 2-D grid, the spherical distribution volume has to be changed to a cylindrical volume as shown in Fig. 2a. This is the case with most of the 2-D non-homogeneous systems.

The thermodynamic property variations along the y-axis is considered unchanged over long period of time and hence the $r(x, z)$ depends only on x and z . The resulting 2-D weight function will follow:

$$\int_{R^3} w(r) dr^3 = \int_0^{r_s} 2\pi r D C_1 [1 - 3r^2/r_s^2 + 2r^3/r_s^3] dr = 1 \quad [11]$$

Here, D is the depth of the system along Y (direction of homogeneity) as shown in Fig. 2a, r_s is the spread radius and the constant of integration is $C_1 = 10/3\pi D r_s^2$.

Figure 2b shows the variation of bond function for a pair of atoms in the case of 2-D system kept at 1.5 nm apart. The isometric view shows the variation of magnitude of bond function for a spread radius of 0.5 nm.

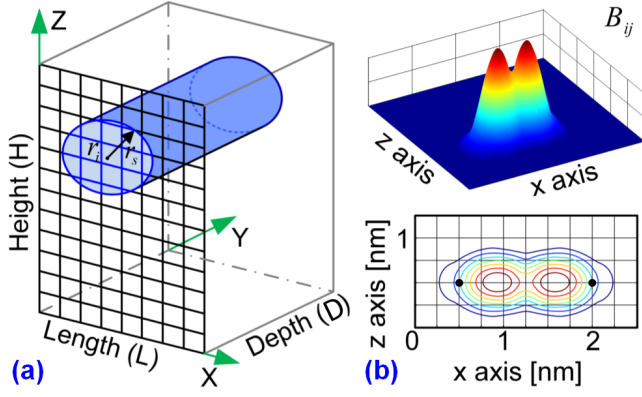


Fig. 2. Weight and bond function developed for 2-D pressure formulation. (a) Cylindrical volume of influence associated with an atom located at , where is the spread radius, L, D, H are length, depth and height respectively. (b) Visualization of bond function for two atoms separated at a distance of 1.5 nm. The gradient image (upper) shows variation along surface and the contour plot of the same is shown below.

Thus, based on the new weight function, the density of the system (ρ) is defined as:

$$\rho(r_p) = \sum_{i=1}^N m_i \hat{w}(r_i - r_p) \quad [12]$$

local number density at a grid point is

$$n(r_p) = \sum_{i=1}^N \hat{w}(r_i - r_p) \quad [13]$$

and temperature as

$$T(r_p) = \sum_{i=1}^N \frac{m_i v_i \otimes v_i}{3n(r_p)k_B} \hat{w}(r_i - r_p) \quad [14]$$

The selection of our interpolation function is arbitrary to demonstrate the 2-D formulation and instead any of the popular functions can be used. With that in mind, we have formulated 2-D forms for some selected functions, along with their 3-D functions are shown below.

Quadratic:

$$\hat{w}_{3D}(r) = \frac{15(1 - r^2/r_s^2)}{8\pi r_s^3} \quad [15]$$

$$\hat{w}_{2D}(r) = \frac{2(1 - r^2/r_s^2)}{D\pi r_s^2} \quad [16]$$

Exponential:

$$\hat{w}_{3D}(r) = \frac{2.2671}{r_s^3} \exp\left(\frac{r_s^2}{r^2 - r_s^2}\right) \quad [17]$$

$$\hat{w}_{2D}(r) = \frac{2.1435}{Dr_s^2} \exp\left(\frac{r_s^2}{r^2 - r_s^2}\right) \quad [18]$$

Trigonometric:

$$\hat{w}_{3D}(x, y, z) = \frac{1}{8r_s^3} \left(1 + \cos\left(\frac{\pi x}{r_s}\right)\right) \left(1 + \cos\left(\frac{\pi y}{r_s}\right)\right) \left(1 + \cos\left(\frac{\pi z}{r_s}\right)\right) \quad [19]$$

$$\hat{w}_{2D}(x, z) = \frac{1}{4Dr_s^2} \left(1 + \cos\left(\frac{\pi x}{r_s}\right)\right) \left(1 + \cos\left(\frac{\pi z}{r_s}\right)\right) \quad [20]$$

For grid dependent and finite support weight functions like B-splines, a rectangular prism volume could be used instead of cylindrical volume.

1-D pressure formulation. For completeness, we have also derived the 1-D variation of pressure and density which is very suitable for 1-D inhomogeneous systems like pressure in thin films, lipid bilayers etc. The $r(z)$ will now depend only on the z-axis and the x and y axis variations are assumed to be negligible over time.

$$\int_{R^3} w(r) dr^3 = \int_0^{r_s} 2LDC_1 [1 - 3r^2/r_s^2 + 2r^3/r_s^3] dr = 1 \quad [21]$$

This will give the integration constant as $C_1 = 1/LDr_s$. This is also consistent with the derivation of Hardy stress (19) and will be shown with example results in the next section.

Results and discussion. In order to demonstrate and validate the new 2-D pressure formulation, we apply it to study the pressure, surface tension and density variations of argon liquid films suspended in argon vapor using MD simulations. In our chosen example (argon liquid film suspended in vapor as shown in Fig. 3a) and also for lipid bilayer (14), the inhomogeneity is in two dimensions (say, X and Z axes) and there is no bulk density variation along the third dimension (Y axis) over ensemble average.

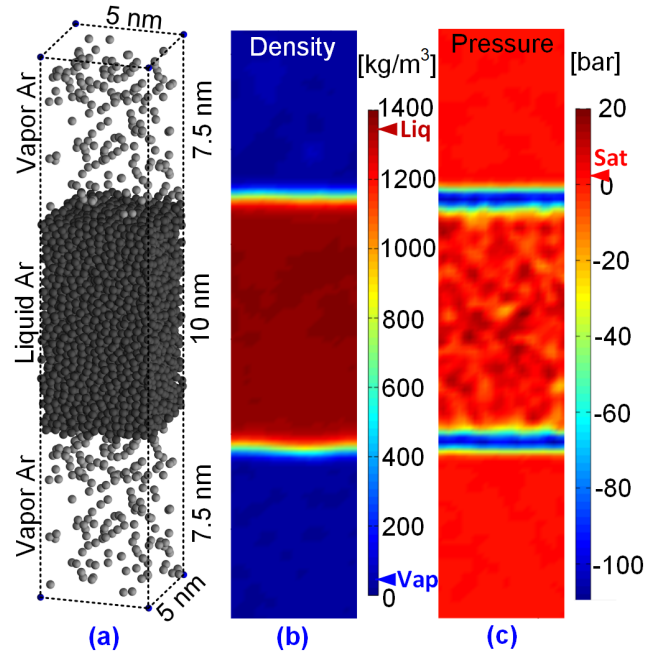


Fig. 3. Two-dimensional density and pressure profile in argon multiphase system using the new 2-D formulation. (a) A 10 nm thick argon film suspended with 7.5 nm thick vapor on both sides along the z-direction. Two-dimensional (b) density and (c) pressure distribution obtained for the system equilibrated at 90 K. The saturation density (NIST data) corresponding to liquid (Liq) and vapor (Vap) are marked in the density plot colorbar, while the saturation pressure (Sat) corresponding to the saturated fluid at 90 K (NIST data) is marked in the pressure plot colorbar showing good agreement with the simulation results.

The computational domain is shown in Fig. 3a. The argon liquid film is 10 nm thick with 7.5 nm thick argon vapor on either side along the z-direction. The X-Y cross section size is 5 nm × 5 nm. Periodic boundary conditions are applied in all directions. The vapor and liquid domains in this molecular system are first equilibrated separately (18) for 1000 ps in order to get a stable suspended film and are then brought

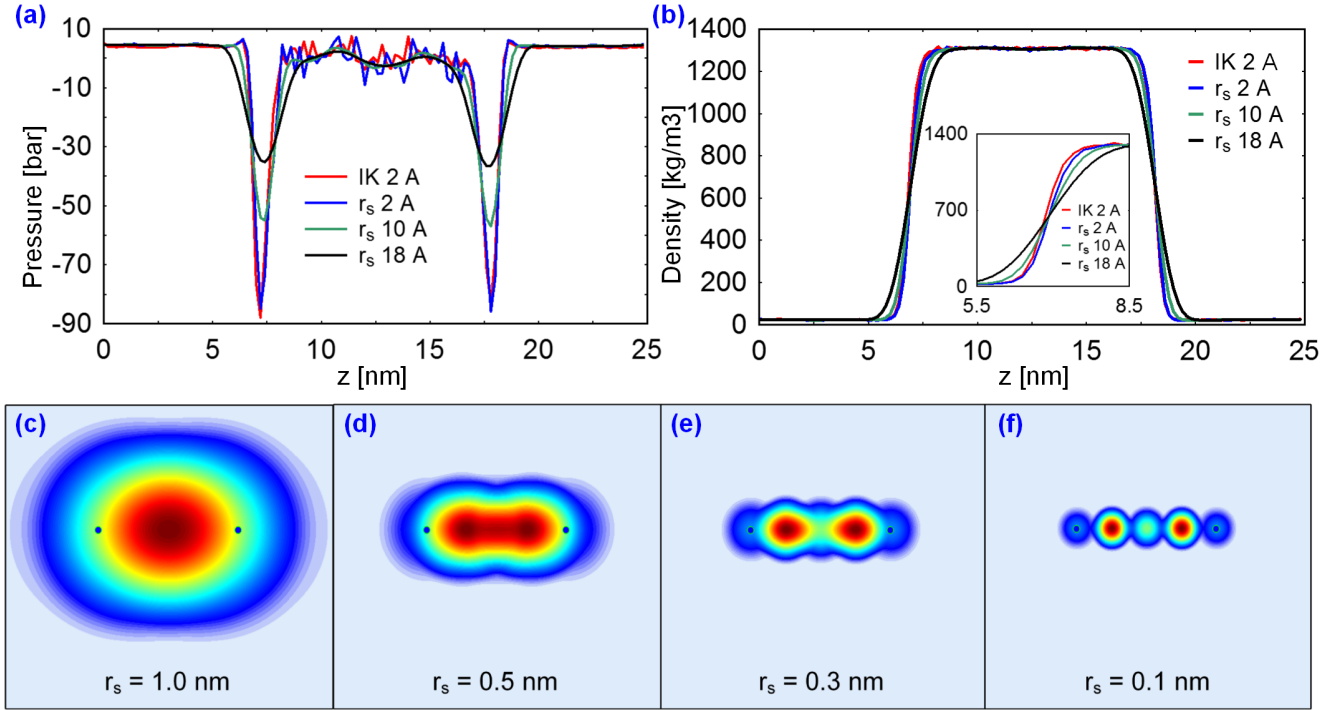


Fig. 4. Sensitivity study of spread radius r_s on bond function, pressure and density. (a) Pressure variation across the argon film for different values of r_s . "IK 2 Å" is the case study using the established Irving-Kirkwood's modified 1-D implementation (18) for comparison. The "IK 2 Å" and the new 2-D formation based profiles show good agreement when the volume of smearing became comparable. (b) Density variation across the film for different values of which confirms that the overall system bulk properties is not affected by the spread radius. (c-f) Contour plots of bond function with r_s ranging from 1 nm, 0.5 nm, 0.3 nm and 0.1 nm for two atoms kept 1.2 nm apart in a 3 nm \times 3 nm domain. The plots visually show how the bond function controls the spreading of the pressure and density across the grids for different spread radii.

them together. The system is then equilibrated for 1000 ps followed by production run for another 1000 ps on which statistical analysis is performed. The modified Stoddard-Ford LJ potential (37) is used with argon – argon LJ parameters as $\sigma_{Ar-Ar} = 0.34$ nm and $\epsilon_{Ar-Ar} = 1.005841$ kJ/mol. The time step of velocity verlet integration is 5 fs and the thermostat to keep temperature constant is chosen as velocity scaling algorithm. MD simulations for different temperatures, spread radius and cutoff radius were performed. A validated, self-written C++ molecular dynamics code is used for all simulations (9).

It is found that the thermodynamic properties like pressure of argon is best captured by using a cutoff radius of 5σ or greater (38). This corresponds to 1.8 nm for argon and we have used the same for all the simulations presented in this work. In the literature, it is common to consider the cutoff radius r_c of MD simulations and spread radius r_s of local pressure calculation as the same. However, considering same cutoff and spread radius will lead to increased number of grid point influence, increasing the computational cost and also limits the finer local details. Hence, in this work, the dependency between spread radius and cutoff radius is removed and considered them as separate entities, which enables us to retain the accuracy of the simulation without introducing any artifacts by choosing a higher cutoff radius. Therefore, the spread radius can be adjusted to capture the localized effects as desired.

Using the developed 2-D formulation, the temporally averaged 2-D contours of density and pressure at 90 K are estimated and shown in Figs. 3b and 3c. The density and

pressure results are compared with the saturation properties from NIST thermodynamic properties database (39) and found to be in very good agreement, which highlights the accuracy of the pressure and density calculation in the new formulation.

The sensitivity of spread radius on pressure and density results is studied using the system shown in Fig. 3a by varying the spread radius to 0.2 nm, 1 nm and 1.8 nm and estimating the 2-D properties of pressure and density. The 2-D values are then averaged along the axis to obtain a 1-D pressure and 1-D density profile varying along the z-direction as shown in Figs. 4a and 4b respectively. Alongside, the pressure and density calculation based on the already-established 1-D IK method (18) with a slab thickness of 0.2 nm are also plotted. The results in Figs. 4a and 4b show that density and pressure smoothen and spreads to a larger area as the spread radius is increased. Also, when the spread radius is small and comparable to the slab thickness of IK method, both density and pressure matches very well. As expected, the bulk region (vapor only and liquid only) properties are found to be not sensitive to the spread radius since it primarily captures the local effects.

Further, to understand the dependency of the bond function to the spread radius, the bond function for two atoms placed at 1.5 nm apart are plotted with varying spread radius of 1 nm, 0.5 nm, 0.3 nm and 0.1 nm (Figs. 4c-f). The resulting images show an important result: the spread radius determines the degree of sharpness required to capture the local features as desired. Further, as long as the integral of bond function is unity and conserved, it does not give erroneous values for surface tension, density or pressure. However, care should

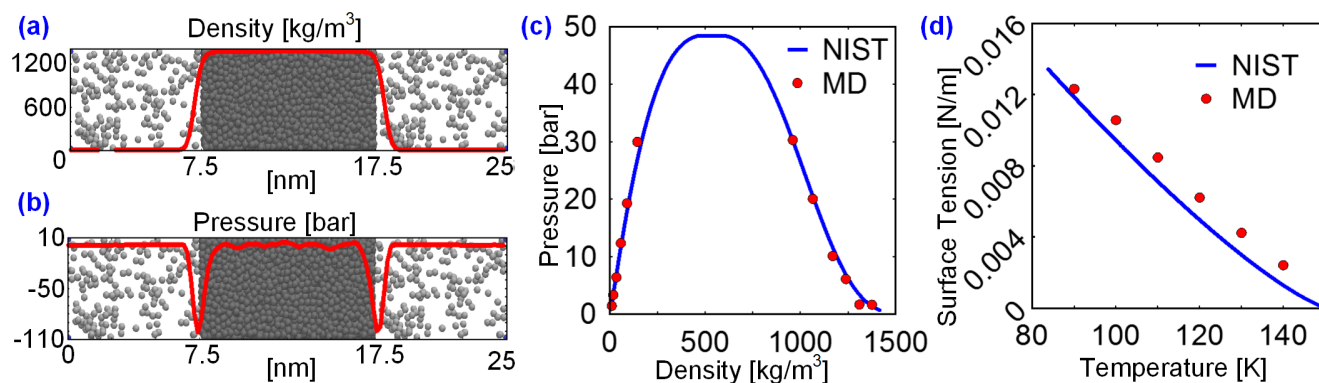


Fig. 5. Comparison of MD simulation results with the standard thermodynamic physical data from NIST (39). (a) 1-D density profile and (b) 1-D pressure profile, deduced from the new 2-D formulation method, plotted over the molecular simulation of argon film. The interface locations capture the expected change in pressure and density. Comparison of MD simulation results and thermodynamic data for (c) pressure vs. density, and (d) surface tension vs. temperature showing excellent agreement. Pressure is estimated by temporal and spatial averaging of vapor and liquid regions separately.

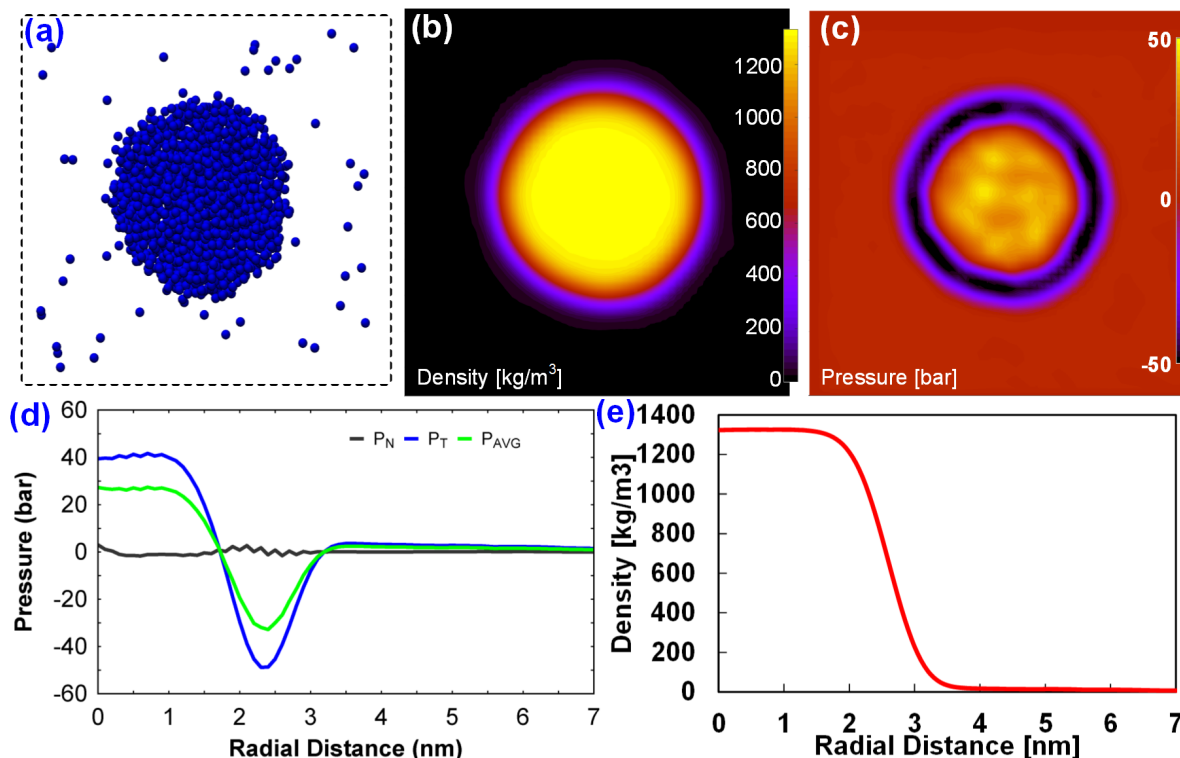


Fig. 6. Laplace pressure study in a cylindrical liquid argon droplet. (a) Molecular model of cylindrical argon in a 3-D periodic box. (b) Density of the system after ensemble averaging using our 2-D method. (c) Pressure of the system ensemble averaged using our 2-D method. (d, e) Pressure and density variation in the cylindrical Argon system using cylindrical coordinate conversion.

be taken while selecting the grid cell size for smearing as the results may be less accurate when the spread radius becomes comparable to grid size (although the resulting artifacts can possibly be alleviated using finite support weight functions like B-Splines, which however needs further investigation).

Next, we validate the 2-D pressure formulation by performing multiple simulations with varying temperature of the argon system (90 K, 100 K, 110 K, 120 K, 130 K, and 140 K) and comparing the simulation results with the experimental thermodynamic properties of argon from NIST database (39). The spread radius and cutoff radius are chosen as 0.5 nm and 1.8 nm respectively for these simulations. We would like re-emphasize the fact that spread radius does not alter any continuum level quantities and the choice of 0.5 nm as the spread radius is merely arbitrary. Thermodynamic quantities of pressure, density and surface tension are estimated using the developed 2-D methodology. The 2-D results are averaged along the x-direction to obtain a 1-D pressure and 1-D density profile varying along the z-direction. A visualization of pressure and density variation along the height of the domain is shown in Fig. 5a and 5b which is consistent with previous argon film studies (17, 18). The comparison of pressure vs. density and surface tension vs. temperature are plotted in Figs. 5c and 5d, respectively, and show very good agreement with the experimental data (39).

Since the above system is inhomogeneous only in one-dimension, we performed another validation on a curvilinear system which is inhomogeneous in two-dimensions. We estimate the pressure difference in a cylindrical droplet as shown in Fig. 6a, and compare the result with the classical Young-Laplace equation. The droplet is symmetric in the plane of the figure with a depth of 3 nm and has periodic boundary conditions in all directions with sides of 11 nm each. The droplet is equilibrated for 1000 ps and then production runs are done for another 2000 ps. The pressure and density is estimated at every 20 steps and averaged using the method introduced in this work. However, during the course of the simulation, the center of the droplet may vary around the original location. In order to avoid a skewed averaging, center of mass of every data set is found and readjusted to the center of the domain before averaging. The resulting ensemble averaged density and pressure is shown in Figs. 6b and 6c respectively. The variation of the pressure and density from the center of the droplet towards outside is shown in Figs. 6d and 6e.

The excess pressure inside the drop is given by the classical Young-Laplace equation:

$$P_{in} - P_{out} = \frac{2\gamma}{R} \quad [22]$$

where P_{out} and P_{in} are the outside and inside pressures of the drop, γ is the surface tension, and R is the radius of the drop. The radius R is estimated by identifying the interface using our interface detection algorithm (40–42). All parameters in Eq. (22) are estimated independently from the MD simulations. For the system simulated, we obtain from the density profile, and the surface tension is estimated. In order to estimate the radial variation of the properties like normal pressure, density, tangential pressure and surface tension, we used the 2-D rotation matrix in combination with B-spline interpolation polynomials. The left hand side of Eq. (22) results in a value of 3.3 MPa, while the right hand side results in 2.5 MPa, and thus, is in good agreement with the Young

Laplace equation. We expect the agreement to improve further for larger drop sizes (however, with added computational cost). These simulations confirm the validity and accuracy of the new 2-D formulation method developed and presented in this work.

Conclusions. In conclusion, a grid based method for two-dimensional estimation of pressure and density was developed and validated. The methodology was applied to a suspended argon liquid film in argon vapor with varying temperatures, and results were in very good agreement NIST experimental database values. The method was also applied to the classical problem of pressure difference calculation in a cylindrical drop and the results were found to be in good agreement with the Young Laplace equation. Further, the dependency between spread radius and cutoff radius was disconnected which allows for high accuracy of the simulation by choosing a higher cutoff radius without introducing any artifacts. The spread radius can be adjusted to capture the localized effects in the system as desired. The developed method will be significantly faster (computationally) than the existing 3-D grid method, and can be very useful in determining stresses occurring in lipid bilayers and other systems where inhomogeneity exists only in two of the three dimensions. This work also supports the fact that for the conversion of virial stress to a continuum level property, both kinetic component and force component of virial stress should be considered.

Nomenclature

1-D	One-dimensional
2-D	Two-dimensional
3-D	Three-dimensional
B_{ij}	Bond function between i^{th} and j^{th} atoms
C_1	Constant of integration
D	Depth
F_{ij}	Force between i^{th} and j^{th} atoms
H	Height
IK	Irving-Kirkwood
L	Length
LJ	Lennard Jones
MD	Molecular Dynamics
N	Number of atoms
P	Pressure
P_{in}	Pressure inside cylindrical drop
P_K	Kinetic component of pressure
P_{out}	Pressure outside cylindrical drop
P_V	Virial component of pressure
R	Radius of cylindrical drop
T	Temperature
k_B	Boltzmann constant
kJ	kilo Joules
m_i	Mass of i^{th} atom
n	Number density of atoms in p^{th} grid point
nm	nano meter
ps	pico second
r_i	Position coordinate of i^{th} atom
r_p	Position coordinate of p^{th} grid point
r_s	Spread radius
r_c	Cutoff radius
v_i	Velocity of i^{th} atom
w	Weight function
ρ	Density
λ	Dummy integration variable
δ	Dirac Delta function
ϵ	Lennard Jones energy well depth
σ	Lennard Jones zero energy distance

Acknowledgment. We acknowledge Prof. Xiantao Li of Penn State University for sharing computer code snippets and the helpful discussions with Dr. Maroo.

1. Horstemeyer MF (2009) Multiscale modeling: a review in *Practical aspects of computational chemistry*. (Springer), pp. 87–135.
2. Lindahl E, Edholm O (2000) Spatial and energetic-entropic decomposition of surface tension in lipid bilayers from molecular dynamics simulations. *The Journal of Chemical Physics* 113(9):3882–3893.
3. Tieleman DP, Marrink SJ, Berendsen HJ (1997) A computer perspective of membranes: molecular dynamics studies of lipid bilayer systems. *Biochimica et Biophysica Acta (BBA)-Reviews on Biomembranes* 1331(3):235–270.
4. Berger O, Edholm O, Jähnig F (1997) Molecular dynamics simulations of a fluid bilayer of dipalmitoylphosphatidylcholine at full hydration, constant pressure, and constant temperature. *Biophysical journal* 72(5):2002–2013.
5. Feller SE, Pastor RW (1999) Constant surface tension simulations of lipid bilayers: the sensitivity of surface areas and compressibilities. *The Journal of chemical physics* 111(3):1281–1287.
6. Steinhäuser M (2008) Computational multiscale modeling of solids and fluids—theory and applications.
7. YD S, Maroo SC (2015) Surface-heating algorithm for water at nanoscale. *The journal of physical chemistry letters* 6(18):3765–3769.
8. YD S, Maroo SC (2016) Origin of surface-driven passive liquid flows. *Langmuir* 32(34):8593–8597.
9. Daisy SY (2016) Ph.D. thesis (Syracuse University).
10. Ollila OS, et al. (2009) 3d pressure field in lipid membranes and membrane-protein complexes. *Physical review letters* 102(7):078101.
11. Sonne J, Hansen FY, Peters GH (2005) Methodological problems in pressure profile calculations for lipid bilayers. *The Journal of chemical physics* 122(12):124903.
12. Lindahl E, Edholm O (2000) Spatial and energetic-entropic decomposition of surface tension in lipid bilayers from molecular dynamics simulations. *The Journal of Chemical Physics* 113(9):3882–3893.
13. Heyes D, Smith E, Dini D, Zaki T (2011) The equivalence between volume averaging and method of planes definitions of the pressure tensor at a plane. *The Journal of chemical physics* 135(2):024512.
14. Vanegas JM, Torres-Sánchez A, Arroyo M (2014) Importance of force decomposition for local stress calculations in biomembrane molecular simulations. *Journal of chemical theory and computation* 10(2):691–702.
15. Yang JZ, Wu X, Li X (2012) A generalized irving-kirkwood formula for the calculation of stress in molecular dynamics models. *The Journal of chemical physics* 137(13):134104.
16. Torres-Sánchez A, Vanegas JM, Arroyo M (2015) Examining the mechanical equilibrium of microscopic stresses in molecular simulations. *Physical review letters* 114(25):258102.
17. Lee SH (2012) Pressure analyses at the planar surface of liquid-vapor argon by a test-area molecular dynamics simulation. *Bulletin of the Korean Chemical Society* 33(9):3039–3042.
18. Weng JG, Park S, Lukes JR, Tien CL (2000) Molecular dynamics investigation of thickness effect on liquid films. *The Journal of Chemical Physics* 113(14):5917–5923.
19. Hardy RJ (1982) Formulas for determining local properties in molecular-dynamics simulations: Shock waves. *The Journal of Chemical Physics* 76(1):622–628.
20. Yesudasan S, Wang X, Averett RD (2018) Molecular dynamics simulations indicate that deoxyhemoglobin, oxyhemoglobin, carboxyhemoglobin, and glycated hemoglobin under compression and shear exhibit an anisotropic mechanical behavior. *Journal of Biomolecular Structure and Dynamics* 36(6):1417–1429.
21. Yesudasan S, Wang X, Averett RD (2018) Fibrin polymerization simulation using a reactive dissipative particle dynamics method. *Biomechanics and Modeling in Mechanobiology* pp. 1–15.
22. Yesudasan S, Douglas SA, Platt MO, Wang X, Averett RD (2018) Molecular insights into the irreversible mechanical behavior of sickle hemoglobin. *Journal of Biomolecular Structure and Dynamics* pp. 1–12.
23. Yesudasan S, Wang X, Averett RD (2018) Coarse-grained molecular dynamics simulations of fibrin polymerization: effects of thrombin concentration on fibrin clot structure. *Journal of molecular modeling* 24(5):109.
24. Irving J, Kirkwood JG (1950) The statistical mechanical theory of transport processes. iv. the equations of hydrodynamics. *The Journal of chemical physics* 18(6):817–829.
25. Hardy RJ, Root S, Swanson DR (2004) Two dimensional continuum properties from molecular dynamics simulations in *AIP Conference Proceedings*. (AIP), Vol. 706, pp. 217–220.
26. Zhou M (2003) A new look at the atomic level virial stress: on continuum-molecular system equivalence in *Proceedings of the Royal Society of London A: Mathematical, Physical and Engineering Sciences*. (The Royal Society), Vol. 459, pp. 2347–2392.
27. Zimmerman JA, et al. (2004) Calculation of stress in atomistic simulation. *Modelling and simulation in materials science and engineering* 12(4):S319.
28. Gall K, Diao J, Dunn ML (2004) The strength of gold nanowires. *Nano Letters* 4(12):2431–2436.
29. Buehler MJ, Gao H (2006) Dynamical fracture instabilities due to local hyperelasticity at crack tips. *Nature* 439.
30. Gates T, Odegard G, Frankland S, Clancy T (2005) Computational materials: multi-scale modeling and simulation of nanostructured materials. *Composites Science and Technology* 65(15):2416–2434.
31. Murdoch AI (2007) A critique of atomistic definitions of the stress tensor. *Journal of elasticity* 88(2):113–140.
32. Subramaniyan AK, Sun C (2008) Continuum interpretation of virial stress in molecular simulations. *International Journal of Solids and Structures* 45(14):4340–4346.
33. Admal NC, Tadmor EB (2010) A unified interpretation of stress in molecular systems. *Journal of elasticity* 100(1):63–143.
34. Zimmerman JA, Jones RE, Templeton JA (2010) A material frame approach for evaluating continuum variables in atomistic simulations. *Journal of Computational Physics* 229(6):2364–2389.
35. Dirac PAM (1981) *The principles of quantum mechanics*. (Oxford university press) No. 27.
36. Welling U, Germano G (2011) Efficiency of linked cell algorithms. *Computer Physics Communications* 182(3):611–615.
37. Stoddard SD, Ford J (1973) Numerical experiments on the stochastic behavior of a lennard-jones gas system. *Physical Review A* 8(3):1504.
38. Weng JG, Park S, Lukes JR, Tien CL (2000) Molecular dynamics investigation of thickness effect on liquid films. *The Journal of Chemical Physics* 113(14):5917–5923.
39. Lemmon E, McLinden M, Friend D (2005) Thermophysical properties of fluid systems, nist chemistry webbook, nist standard reference database. *WGMFJ Linstrom, Eds* 69.
40. Daisy SY, Maroo SC (2017) A robust algorithm for contact angle and interface detection of water and argon droplets. *Heat Transfer Engineering* 38(14-15):1343–1353.
41. Yd S, Maroo SC (2015) A new algorithm for contact angle estimation in molecular dynamics simulations in *ASME 2015 13th International Conference on Nanochannels, Microchannels, and Minichannels collocated with the ASME 2015 International Technical Conference and Exhibition on Packaging and Integration of Electronic and Photonic Microsystems*. (American Society of Mechanical Engineers), pp. V001T04A007–V001T04A007.
42. Yesudasan Daisy S (2015) An efficient algorithm for contact angle estimation in molecular dynamics simulations. *International Journal of Engineering* 9(1):1–8.